Article

Innovative Tool for Automatic Detection of Arterial Stenosis on Cone Beam Computed Tomography

Agnese Simoni [1,2,†], Eleonora Barcali [1,3,†], Cosimo Lorenzetto [2], Eleonora Tiribilli [1,2], Vieri Rastrelli [3], Leonardo Manetti [2], Cosimo Nardi [3,*], Ernesto Iadanza [4,‡] and Leonardo Bocchi [1,‡]

1   Department of Information Engineering, University of Florence, v. Santa Marta, 50139 Florence, Italy
2   Epica Imaginalis, Via Rodolfo Morandi 13/15, 50019 Sesto Fiorentino, Italy
3   Department of Biomedical Experimental and Clinical Sciences "Mario Serio", University of Florence, 50139 Florence, Italy
4   Department of Medical Biotechnologies, Via Aldo Moro 2, 53100 Siena, Italy
*   Correspondence: cosimo.nardi@unifi.it
†   These authors contributed equally to this work.
‡   These authors contributed equally to this work.

Abstract: Arterial stenosis is one of the main vascular diseases that are treated with minimally invasive surgery approaches. The aim of this study was to provide a tool to support the medical doctor in planning endovascular surgery, allowing the rapid detection of stenotic vessels and the quantification of the stenosis. Skeletonization was used to improve vessels' visualization. The distance transform was used to obtain a linear representation of the diameter of critical vessels selected by the user. The system also provides an estimate of the exact distance between landmarks on the vascular tree and the occlusion, important information that can be used in the planning of the surgery. The advantage of the proposed tool is to lead the examination on the linear representation of the chosen vessels that are free from tortuous vascular courses and from vessel crossings.

Keywords: cone beam computed tomography; segmentation; stenosis; software

1. Introduction

Image-guided surgical navigation is one of the main technologies used for minimally invasive surgery, which, in turn, is a technique that introduces several advantages over traditional open surgery. This reduces the size and number of incisions that need to be made on the body of the patients, inducing a faster recovery of the patient and a reduced risk of injury-related complications, as well as lower hospitalization costs [1]. On the other hand, minimally invasive surgery often requires computed tomography (CT) and/or magnetic resonance imaging (MRI) of the anatomical area to be combined with the operating scenario. In this context, surgical planning acquires a decisive role as the best outcomes are achieved when surgeons are preoperatively prepared with a deep understanding of the anatomy they will face. To obtain an accurate model of the anatomical part that needs to be studied, some steps need to be performed. First, high-quality images of the anatomical structures of interest must be acquired, followed by segmentation of the parts of interest and rendering the surface or volume using specialized software [2,3]. The resulting models allow the surgeon to observe the anatomy from different angles and define the best-possible route to reach the area of interest [4,5]. The realization of models before surgery is spreading more and more. It allows not only the surgeon to gain an idea and act in a more targeted way, but also students to practice and learn techniques of intervention [6]. Hoetznecker et al. in their work realized a color-coded 3D model of benign glotto-subglottic stenosis and a control airway using a commercial 3D printer starting from CT scans. They showed how the realization of a 3D model resulted in being the more accurate diagnostic strategy compared to the endoscopy and the CT scan usually used for these diagnoses [7]. Furthermore,

Shi et al. showed, as the application of a preoperative planning software to treat the lumbar foraminal stenosis, advantages such as the reduced puncture channel establishment time, operative time, and number of intraoperative fluoroscopic images taken without affecting the clinical outcomes [8]. Marragianis et al. showed the possibility of making patient-specific models of the anatomic and functional characteristics of severe aortic valve stenosis using 3D stereolithographic printing to convert high-resolution CT images into life-sized physical models. The CT digital data were processed with a computer-aided design (CAD) software and exported to a multi-material 3D printer to create dual-material fused 3D models of severe aortic stenosis. The realized model accurately reflected the anatomy with excellent visual correlation to the corresponding clinical CT. The possibility of obtaining specific tailored models can lead to further advances in surgery [9]. Our study focused on the applications of the 3D model in the field of endovascular surgery, a branch of minimally invasive surgery, with the aim of restoring natural blood flow in pathological conditions affecting the vascular system such as the occluded arteries. Numerous diseases, as well as aging induce pathological changes in vascular structures. One of the most-common alterations consists of a reduction in the diameter of the the vessel, resulting in stenosis of varying severity up to a complete occlusion; this type of alteration leads to changes in blood flow, thus reducing the supply of the normal amount of oxygen-rich blood to the tissues, eventually leading to serious complications [10,11]. For this reason, the study of the properties of the arterial walls is the subject of several papers, as well as providing important information that can increase the performance of doctors in both the diagnosis and therapy of vascular pathology [12–17].

The purpose of this study was the development of a new vessel analysis tool that supports the endovascular surgeon in preoperative planning; in particular, it performs an analysis of the vascular tree of the area of interest, enabling a rapid localization and quantification of vascular stenosis. The peculiarity of the suggested tool is to conduct the recognition of occlusion directly on the 3D rendering of the vessels, thus helping in the workflow of surgery.

2. Materials and Methods

We analyzed two cone beam computed tomography (CBCT) scans of the chest of a cat, pre- and post-contrast administration, acquired with a VIMAGO scanner (VIMAGO™ HU, Epica Medical) using the following parameters: 9 ms, 90 mA, 80 peak kilo voltage (KVP). Before the second acquisition, a bolus of Lopamiro, 600 mg/kg, was administered to the animal. Both acquisitions were performed by a professional veterinarian for diagnostic purposes. The process for obtaining the 3D rendering of the vessels, the analysis of their diameter, and the stenosis detection follows the steps described in the following paragraphs.

2.1. Segmentation

The first step is the segmentation. Accurate vascular segmentation is crucial as further analysis of vessels' properties depends on the accuracy of this procedure. In this study, we exploited a segmentation algorithm presented in a previous paper by Simoni et al. [18] and briefly summarized below. This algorithm consists of two consecutive steps: bone segmentation and vessel segmentation. The images are acquired with two CBCT scans, carried out before and after the administration of the contrast medium, respectively. The first acquisition is used to segment the bones. This step is necessary to obtain a binary mask to apply on the contrast image. This binary mask improves the segmentation of vessels in the contrast image, avoiding errors related to a similar gray level distribution of bones and vessels with contrast. Thus, segmented vessels are obtained first by subtracting the segmented bones from the image with contrast and, then, applying a second phase of segmentation on the resulting image. Both segmentations are based on a threshold approach (with an empirically selected threshold), which provides provisional segmentation, further refined by a region-growing method, as explained in the following. The region-growing method begins with a seed point, which is determined with the help of a function that is able to identify all spherical shapes in the frame by exploiting the circular Hough transform

(CHT). Then, the method iteratively groups voxels according to a proximity criterion and a predefined acceptance rule. This consists of comparing the voxel under consideration with the seed point: the difference in the gray levels between the seed point and voxels under test must be lower than a certain local threshold, determined empirically. The algorithms used to determine the segmentation of the bone and the vessel are shown, respectively, in Figures 1 and 2.
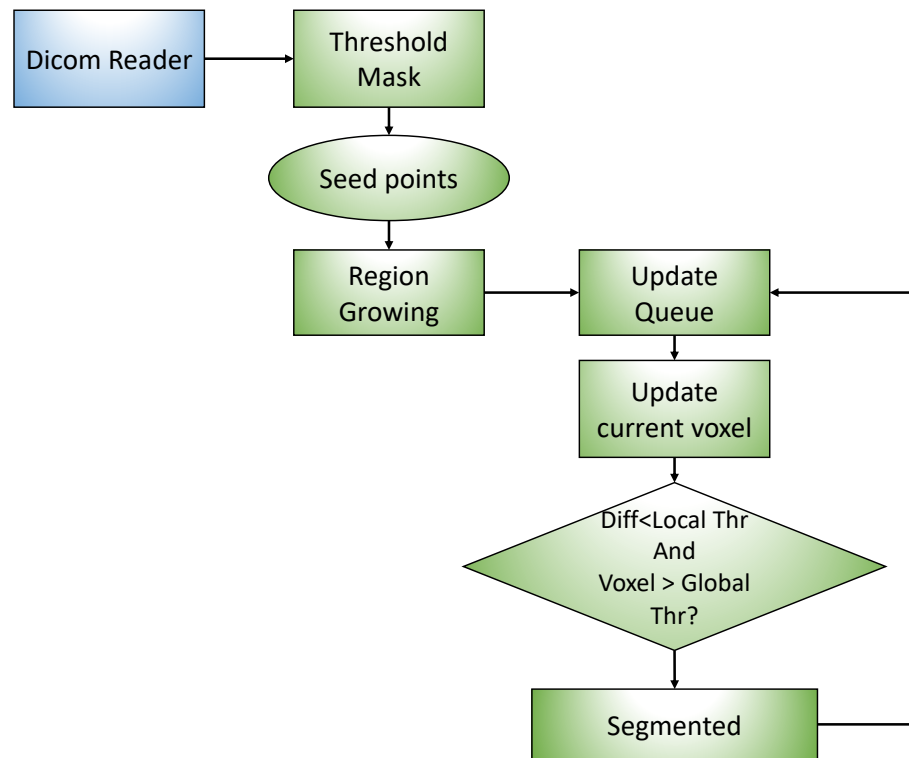

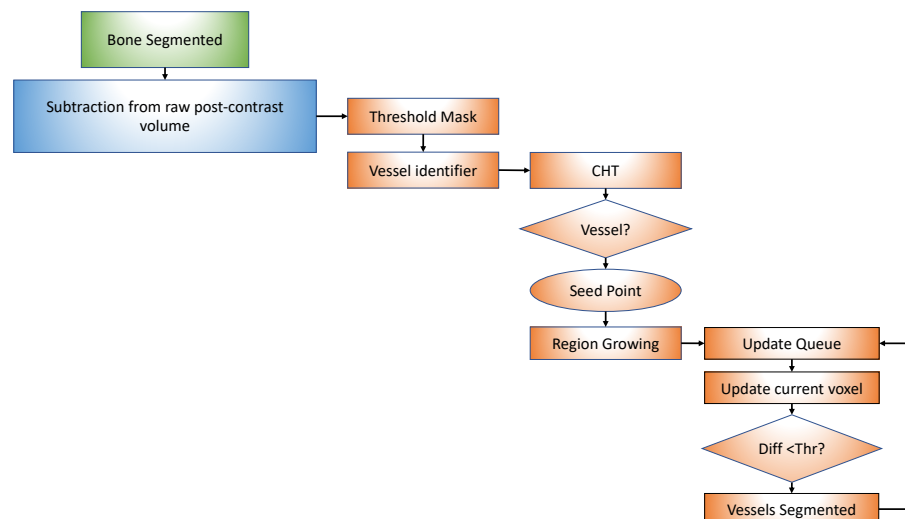**Figure 1.** Overview of the bone segmentation algorithm.

Figure 2. Overview of the blood vessel segmentation algorithm.

2.2. Skeletonization

Skeletonization consists of an iterative process of segmented image thinning, producing centerlines from binary or gray-scale images by extracting medial axes or ridges [19]. The skeleton is a basic representation of the shape of an object that has been reduced to

its minimum level. In this case, it takes the binarized volume as the input and outputs a 3D binary image with the same measurements as the reference binarized volume. Vessel skeletonization is performed through an appropriate function present in MATLAB. The skeletonized vessel tree provides a simplified representation of the complex vascular ramifications and pixels that form it. By reducing the volume of blood vessels to their skeleton, the overlap between vascular segments is eliminated accordingly, increasing the understanding of the flow path followed by the blood. The structure of the skeletonized image is then analyzed with the algorithm developed by Kollmannsberger [20], which, starting from a 3D binary skeleton, produces a topological description of the tree providing the adjacency matrix of the graph and two structures containing information about the nodes (coordinates, list of connections for each node, etc.) and links, respectively. By the term "nodes", we refer to the points of bifurcation where a vessel splits into two smaller vessels, while by "link", the set of points that are on the branch.

2.3. Diameter Analysis

The skeleton is then associated with a local representation of the vessel diameters. The local diameter of the vessel can be estimated with the distance transform function. The distance transform operates on binary images and calculates the distance of each pixel in the foreground from its nearest point in the background. Specifically, it associates the intensity of each pixel with the value of the distance between that pixel under study and the nearest pixel in the background [21]. In our case, the input binary volume of vessels constitutes the foreground, so that each pixel of the resulting image, belonging to the vessels, represents its distance from the vascular lumen. Figure 3a shows an example of a frame of the output volume of the distance transform. We can observe that the intensity of the pixels is higher in the center of the vessels, where the distance from the vascular wall reaches its maximum value, while it gradually decreases near the edge of the vessels. The maximum of the distance transform in each vessel provides an accurate estimate of the vessel radius in the given section. Therefore, we associated each point of the skeleton with the value returned by the distance transform applied to the corresponding complementary of the binary volume of the vessel under examination. At the end of the procedure, each pixel k along each branch of the skeleton i is associated with the corresponding distance transform value $r_{i,k}$, providing information of the diameter of the vessel associated with the skeleton.
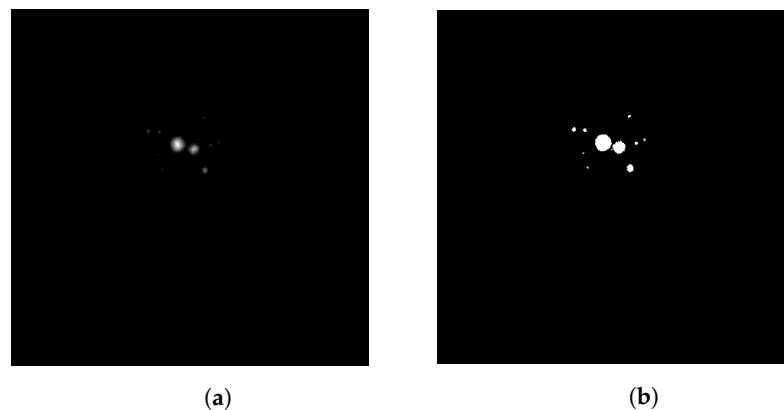

(**a**)   (**b**)

Figure 3. Distance transform. (**a**) Frame of the output image resulting from the application of the distance transform on the binary mask produced by the segmentation of the vessels. (**b**) The corresponding frame of vessels' binary mask.

2.4. User Interface

The proposed tool includes a graphical user interface (GUI) that allows the user to view the analysis results both in 3D and 2D representation. The 3D representation shows the vessel skeleton, color-coded according to the estimated diameter of the vessel, providing the user with explicit information about the thickness of each vessel directly on the 3D representation of the vessels. Each point of each vessel in the tree is painted using a color-

coding scheme based on the classic "jet" colormap, where smaller vessels appear as dark blue; as the diameter grows, these appear lighter up to the larger ones, which appear as bright red. From this representation, the user can select a single vessel composed of several tree segments, for a detailed analysis of the diameter. The procedure begins by selecting the first segment of the vessel, which turns red, while all adjacent segments of the vascular tree are highlighted in green. At this point, the user may select multiple segments, which are consecutively added to the vessel under study. Once a new segment is selected, the representation is updated by drawing all selected segments in red, while the green color identifies the segments that may be further selected for extending the vessel, i.e., segments connected at one of the extremities of the vessel itself.

In order to provide a more detailed view of the variation of the diameter along the selected vessel, the tool also provides a 2D view mode. This two-dimensional plot provides a means to make the search for stenosis more intuitive for medical doctors, compared to the 3D visualization of the skeleton. When the user selects a vessel on the skeleton, the corresponding link and pixels that belong to it are identified and the corresponding linear representation appears, where the horizontal axis represents a linear coordinate L_t along the vessel axis, and the vertical axis indicates the corresponding vessel diameter.

The points on the x-axis are estimated as an integral of the Euclidean distance ΔL_i between each pair of consecutive points in the list describing the structure of the vessel tree. The measure of the diameter of the vessel is obtained by representing, on the y-axis, the value $r_{i,k}$, associated with each pixel of the branch k (or branches) chosen on the skeleton. The plot is also mirrored along the x-axis, to provide a better visual representation of the vessel structure.

The diameter and length of the vessel are scaled in real units (mm) referringto two DICOM tags present in the original pre-contrast CBCT image: the pixel spacing and the slice thickness. The first one is expressed by a pair of values $(\hat{x}, \hat{y})$ that correspond, respectively, to the spacing between the centers of adjacent rows (mm) and the spacing between the centers of adjacent columns (mm) of the image. The other one is represented by $\hat{z}$, which corresponds to the nominal slice thickness measured in mm.

Information about the length of the vessel is obtained as $L_t = \sum_0^t \Delta L_i$, where ΔL_i is computed using the following equation:

$$\Delta L_i = \sqrt{(x_i - x_{i-1})^2 \hat{x}^2 + (y_i - y_{i-1})^2 \hat{y}^2 + (z_i - z_{i-1})^2 \hat{z}^2} \tag{1}$$

where (x_i, y_i, z_i) are the coordinates of the i-th voxel on the axis of the vessel.

As for the vessel diameters, since CBCT scanners acquire isotropic volumes, both DICOM tags have the same value, v. Thus, diameter conversion from pixel units into millimeters is performed by multiplying $r_{i,k}$ by v. In the case of extension to non-isotropic acquisitions, a correct calculation of the diameter of the vessel will require either developing an interpolation strategy for transforming the volumetric image into an isotropic one or the development of a modified distance transform algorithm, taking into account the different scales.

Figure 4 shows the flow chart of the proposed image analysis tool, summarizing both the diameter calculation and visualization.

2.5. Detection of Suspected Stenosis

The system also includes a module for detecting and emphasizing diameter reductions that could be a manifestation of a pathological stenosis. The algorithm employs a moving average filter sliding its window along the segment under study. The filter computes the average radius associated with the pixels contained in each window, rejecting noise and artifacts possibly occurring during image segmentation and diameter estimation. If the difference between the radius of the current pixel and the output of the filter exceeds the fixed threshold, the point is considered as an occlusion of the vessel and brought to the attention of the clinicians. The length of the window was chosen in order to analyze tracts about 1.5 mm long. We chose this value arbitrarily in order to smooth out the noise that may appear in the estimation procedure, while not rejecting small stenoses. However, the

operator can properly tune this value in order to obtain the optimal results. Furthermore, the plot highlights the variations in diameter that occur at vessel bifurcations, where a change in the diameter of the vessel is physiologically plausible.
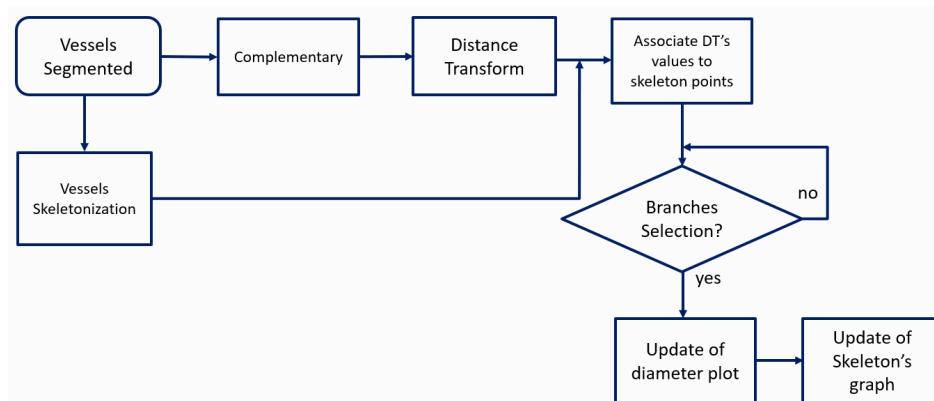

Figure 4. Flow chart of the proposed vessel analysis tool.

To validate the performance of our system, we compared the results detected by our tool with the measurements identified by expert radiologists on the post-contrast CBCT scan DICOM images using an open-source software, Horos™ v3.3.5 software (© 2019, HorosProject).

3. Results

This study provides a tool to facilitate surgeons in detecting arterial stenosis. Critical vessels are identified on the corresponding 3D skeleton of the analyzed CBCT volume, as shown in Figure 5a, where the thickness of each branch is specified. When a branch is selected by the user, the colored skeleton turns gray, while the chosen segment turns red and its consecutive branches turn green, as shown in Figure 5b. Extraction of further vessels follows the same steps as described above. All vessels that have been selected at least once remain red, allowing the user to follow the flow of the vessel under study. This representation is schematized in Figure 5c. Once the skeleton is selected, the two-dimensional plot corresponding to that tract of the segment is also realized, as seen in Figure 5d. The phase of segmentation was previously validated in the paper of Simoni et al., from which we resumed the process to perform our segmentation [18]. They compared the results with the reference images obtained performing a manual segmentation. This analysis showed a sensitivity of 0.748 and a specificity of 0.999.

Our system was able to identify the presence of stenosis in the upper mediastinum at the level of the epiaortic vessels. The value of the stenosis shown in the linear graph is 0.84 mm. This corresponds to a little more than a 50% stenosis of the left subclavian artery. This value was calculated from the y-coordinate measurement of 0.419 mm. Once the user selects the tract of interest, the corresponding linear representation appears. On the plot shown in Figure 6 is reported the two-dimensional representation of the segment and the values of the coordinates x and y. This graph shows contemporaneously the length of the tract along the x-axis and the value of the diameter along the y-axis.

The values on the y-axis are plotted with respect to each point of the skeleton of that branch starting from the values obtained with the distance transform. Specifically, the value of the diameter on the graph is obtained by taking these values and reversing them symmetrically with respect to the x-axis.

Thus, given that the coordinate y on the graph of Figure 6 has value $y = 0.419$ mm, on the y-axis, the diameter is equal to double that value, that is 0.84 mm.

This value was compared with the measurement performed by the radiologists, who identified, on the coronal plane, a diameter of about 1.06 mm, as shown in Figure 7. The relative error between the two estimates corresponds to approximately 20%. These measurements were performed manually using a digital ruler, and thus, as with any other

type of manual measurement, they are subject to human mistakes and inter-individual variability. However, the fact that the values measured both manually and by our tool are approximately similar suggests, first of all, that the system has detected correctly the narrowing point of interest and, secondly, that our tool can improve the accuracy of the human measurements by reducing human subjectivity.

The system is able to detect even minimal narrowing, which might not be visible simply by just the CBCT volume, as shown in the example reported in Figure 8.

The tool has the same ability for both wide and narrow vessels segments, as the detection of structural variations is based on short vessels tracts by comparing the variation of the diameter between the current point and the mean diameter of the analyzed tract.
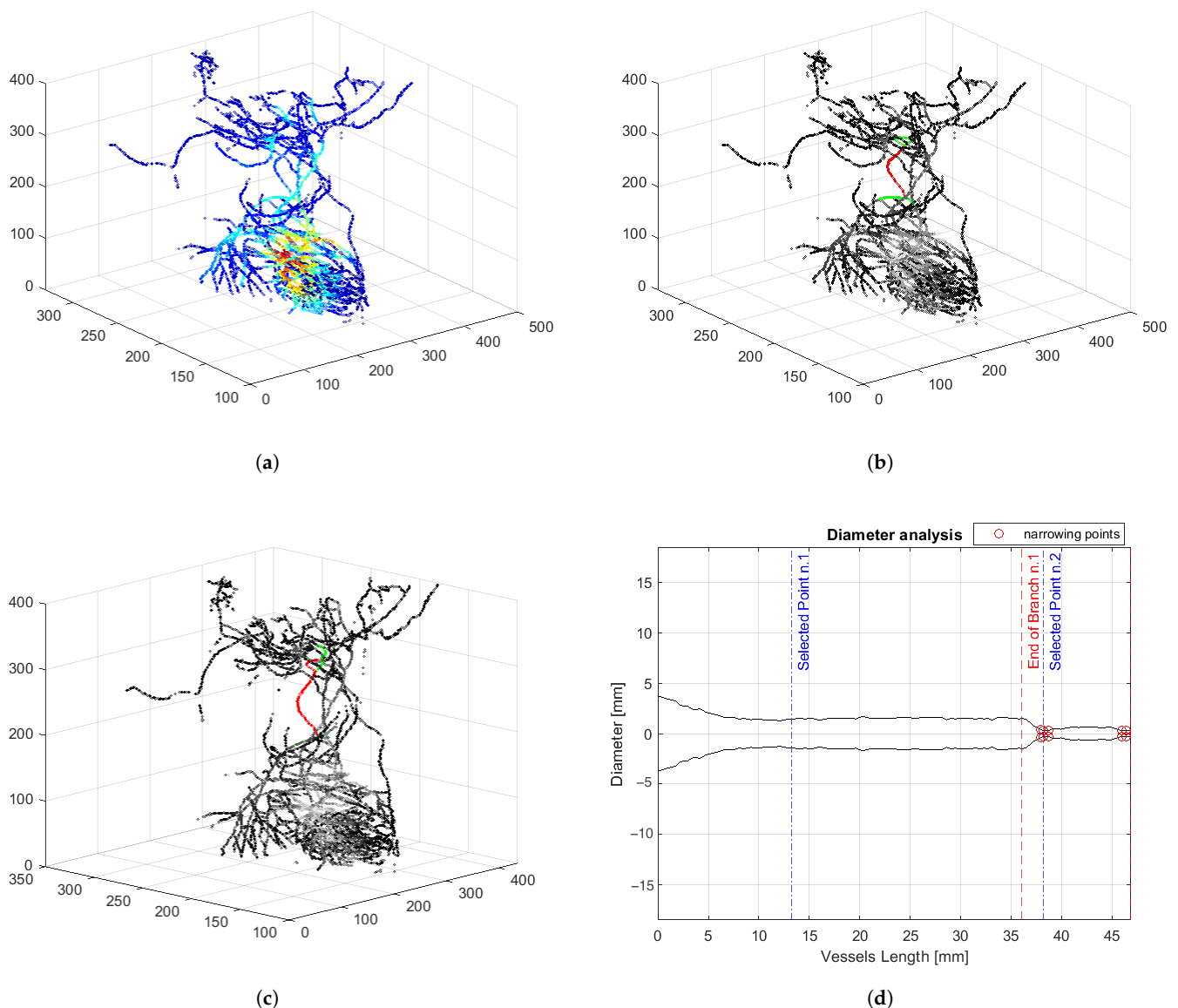

(**a**)

(**b**)

(**c**)

(**d**)

Figure 5. Overview of the vessel analysis tool functioning in response to the selection of two branches on the skeleton. (**a**) Skeleton of the vascular tree. (**b**) After selecting the first branch, the skeleton is shown in gray-scale skeleton, the selected branch is red, and its adjacent segments are green. (**c**) Once the second branch is selected, the GUI shows all selected branches in red and adjacent tracts of the last selected segment in green. (**d**) Linear representation of the vessels.
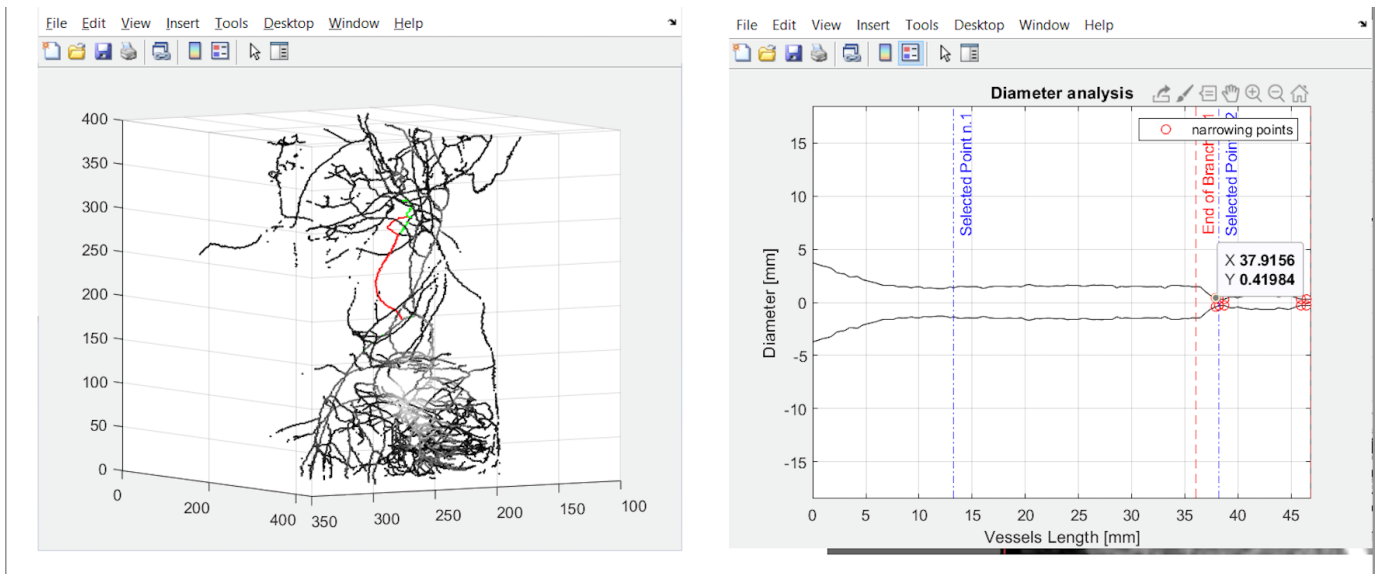
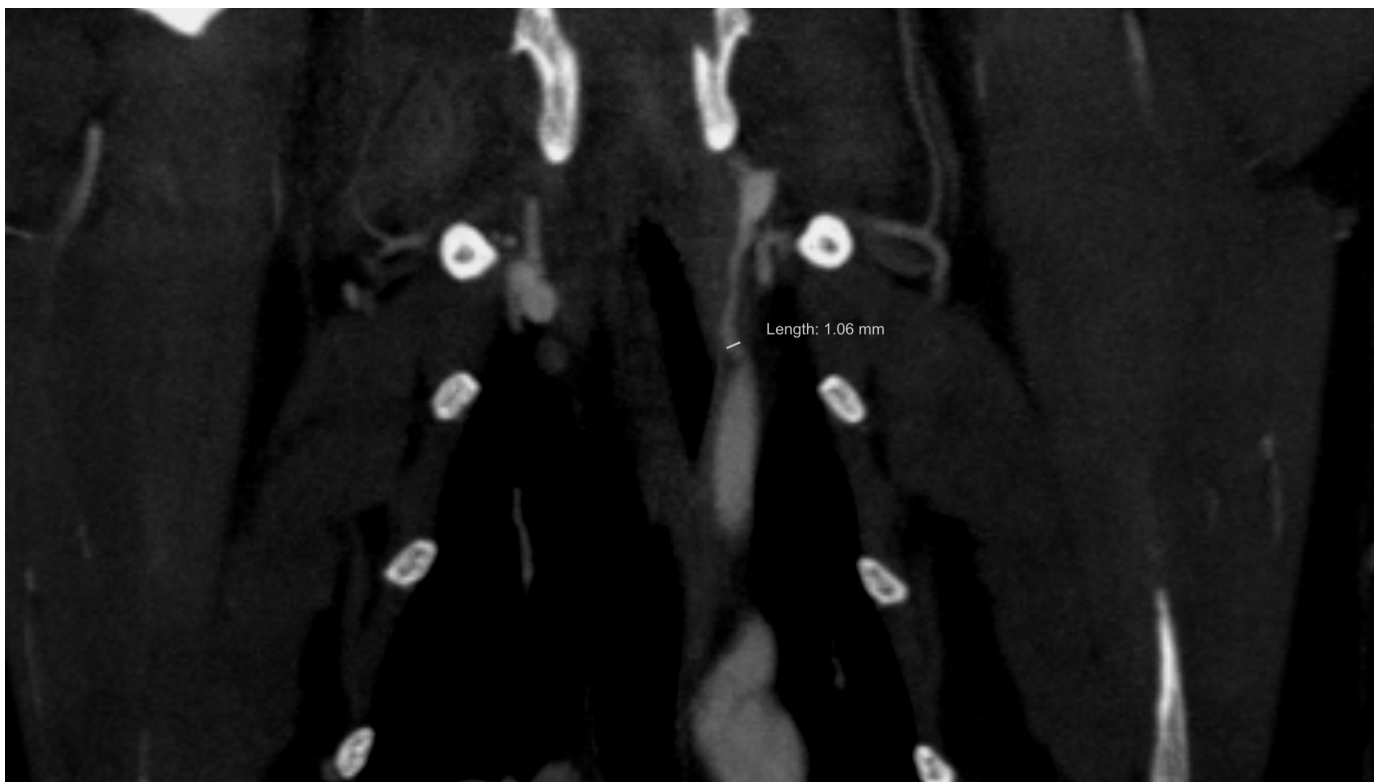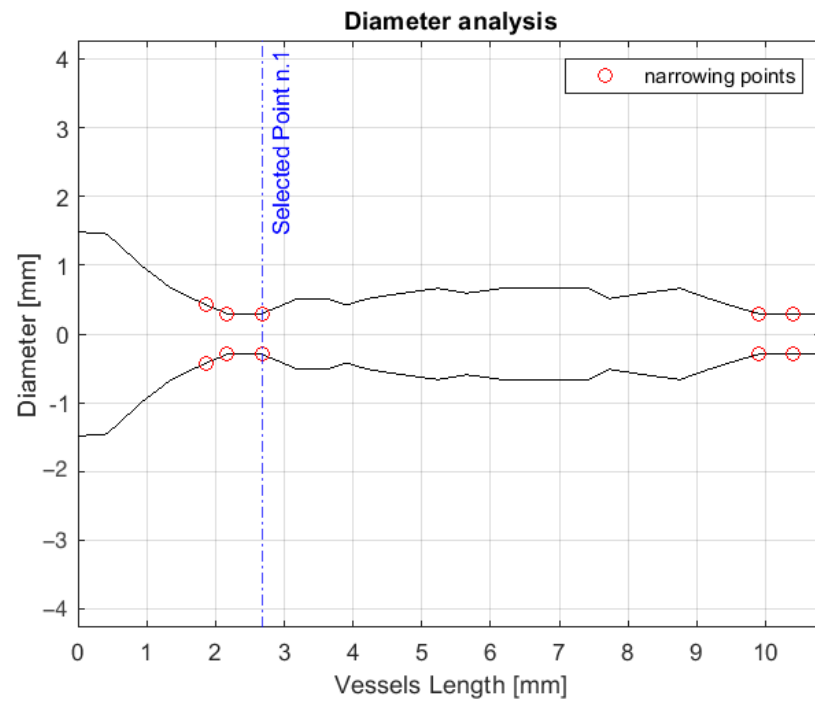**Figure 6.** Skeletonization and linear representation of the tract in which the tool has identified the stenosis.
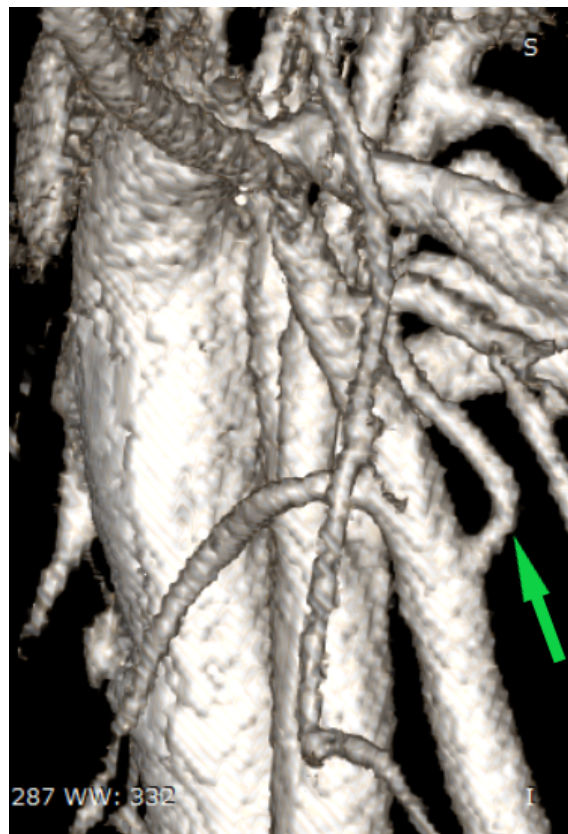

Figure 7. Measurement of the stenosis in the coronal view made by expert radiologists.

(**a**)

(**b**)

Figure 8. (**a**) Linear representation of a vessel presenting five narrowing points that are highlighted with red circles. (**b**) A view of the 3D image of the vascular tree. The green arrow indicates the analyzed vessel in (**a**).

4. Discussion

The proposed system aims to perform an analysis of the vascular tree of the area of interest, supporting the user in the rapid recognition of stenotic branches during preoperative planning. The system contributes to the identification of arterial stenosis, bringing the attention of the clinician to the tracts with suspicious alterations of the vascular lumen. These points are detected by comparing diameter changes along each segment and highlighting narrowing points that exceed the tolerance. The aim of minimally invasive approaches and related tools is to highlight the precision of surgery, improving outcomes such as reducing intraoperative complications and the operative time, and, overall, to improve the safety of the patients. In general, 3D models can be virtual, printed, or augmented reality [22] and are based on high-resolution imaging such as multi-parametric MRI or CT. Vilser et al. introduced a technique for studying the behavior of large retinal vessels using diameter measurements [23], while Heneghan et al. focused on calculating both the tortuosity and the width of the retinal vessels using a morphological processing carried out on segmented vessels [24]. Vascular structural parameters can be exploited in several analysis tools as in the case of Boskamp et al. [25], who developed a software that enriches the visualization of datasets from angiographic CT and MR imaging. The system supplements traditional 2D viewers of the original images with the 3D rendering of the vascular tree, in addition to quantitative morphometric information such as curvature and tortuosity measurements.

The system we realized implements an interactive three-dimensional view of blood vessels, which allows a deepened examination of these anatomical structures by the surgeon. The clinician identifies stenotic points by progressively selecting consecutive blood vessels on the vascular tree rendering. The tool analyzes the chosen segments and emphasizes the tracts that present suspected narrowing, basing the identification of stenotic points on vessels diameter measures obtained with the distance transform technique. It takes advantage of a graphical user interface, which improves the performance of the tool for the user (reported in Figure 9). The GUI presents a section that allows the user to interact with the skeleton of the vascular tree selecting the branches of interest on the skeleton itself. The chosen vascular segments are linearized and represented on a diagram, where the vessel diameter is drawn as a function of vessel length. Moreover, narrowing points, where the vessel diameter drops below a predefined threshold, are highlighted on the plot and brought to the attention of the clinician.
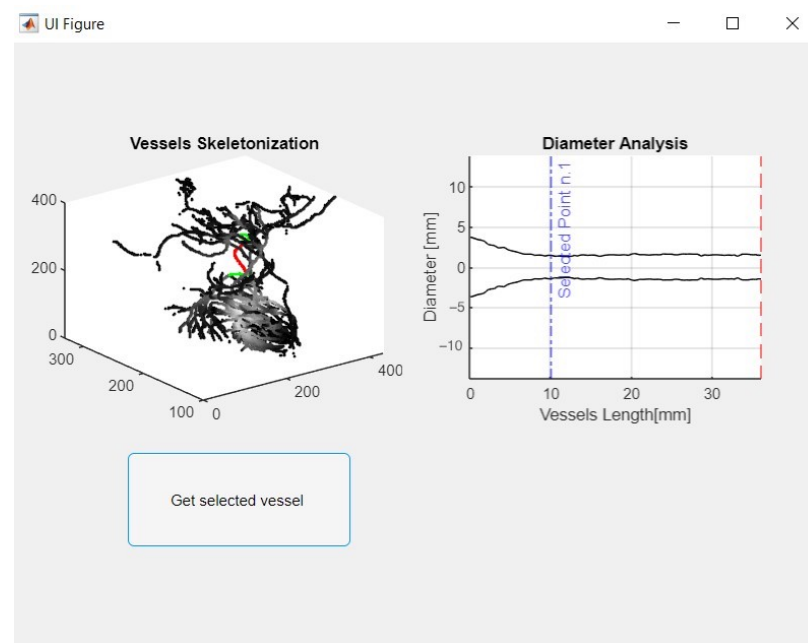

Figure 9. Main window of the system; on the (**left**), 3D plot of the skeletonized vessel tree; on the (**right**), plot of the vessel(s) diameter as a function of length.

The system replaces the complicated 3D rendering of vascular trees with a representation that follows the centerlines of vessels. This "skeletal" image has the advantage of enhancing the bifurcations points and tortuosity of vascular segments, easing the visualization of vascularization and the detection of critical vessels. Vessels are selected by the medical doctor directly on the skeleton. The tool offers a rendered image, which follows the natural course of the vessel under study as its constituent tracts are selected by the user. The skeleton adopts a color code that assists the user in the choice of the segments that are linked to the analyzed vessel, in order to reconstruct the right vascular course. Besides, the surgeon is supported in the identification of stenotic points, as they are marked on the linear representation of the vessel. A further functionality of the vessel analysis tool is allowing the computation of the distance between a reference point on the vascular tree and the point affected by the stenosis. This important clue can be used in the surgical planning phase as it determines the length of the path that will be covered by the catheter during the surgery. At the same time, this information might be used during the surgery, as it has the possibility of reducing the number of angiographic acquisitions that are necessary to control the advancement of the catheter inside the vessel.

We chose to analyze a CBCT volume of the thorax of a cat before and after contrast administration. The system successfully detected the presence of a stenosis of about 50% in the upper mediastinum at the level of the epiaortic vessels.

The advantage of the proposed tool is to lead the examination by the linear representation of the chosen vessels, as shown in Figure 5d, where the vessel is represented as if it were stretched along its length. In fact, the linear representation is free from tortuous vascular courses and vessel crossings, which often increase the effort of clinicians in detecting diameter variations. The limitations of this study include the need for more tests to validate the results, the arbitrariness in the choice of the threshold during the segmentation step, and the problem of vascular enhancement due to the imaging technique used. The problem with the low number of tests is related to the difficulty of recruiting vascular stenosis of animals performed on CBCT scans. Dedicated CBCT scanners are not very popular for studying animals, and it is even more difficult to spot animals with stenotic arteries as collateral findings in examinations carried out for other purposes. Exposing animals to X-rays without a real clinical question is not ethically justified [26]. We are planning to create a simulated test bench for an objective assessment of the proposed algorithm.

The contrast agent needs to be homogeneously distributed to give the correct information. Since CBCT exposure times are longer than traditional multislice CT, there is a risk that the enhancement is not distributed evenly during the whole acquisition and that this can therefore affect the correct display and subsequent segmentation. A solution could be the application of a programmable veterinary infusion pump to administer the contrast agent in order to generate a uniform and prolonged enhancement profile.

5. Conclusions and Future Developments

The results of this study indicate that surgical planning with preoperative 3D imaging of the vessels may potentially reduce the rate of complications during surgeries. Thanks to this system, medical doctors may visualize how the branch tree evolves and the measures by which it is featured. However, larger studies will be needed to confirm these results. In the future, apart from realizing models to test the performance of the algorithm, an extension of this paper could be to implement this system in the environments of virtual and augmented reality, which are experiencing great interest for preoperative planning together with intraoperative navigation, as these technologies can create completely artificial environments, enriching the surgical immersive experience of the team with more available information.

References

1. Cleary, K.; Peters, T.M. Image-guided interventions: Technology review and clinical applications. *Annu. Rev. Biomed. Eng.* **2010**, *12*, 119–142. [CrossRef] [PubMed]

2. Sakamoto, T. Roles of universal three-dimensional image analysis devices that assist surgical operations. *J. Hepato-Biliary-Pancreat. Sci.* **2014**, *21*, 230–234. [CrossRef] [PubMed]

3. Stella, F.; Dolci, G.; Dell'Amore, A.; Badiali, G.; De Matteis, M.; Asadi, N.; Marchetti, C.; Bini, A. Three-dimensional surgical simulation-guided navigation in thoracic surgery: A new approach to improve results in chest wall resection and reconstruction for malignant diseases. *Interact. Cardiovasc. Thorac. Surg.* **2014**, *18*, 7–12. [CrossRef] [PubMed]

4. Tiribilli, E.; Iadanza, E.; Lorenzetto, C.; Manetti, L.; Bocchi, L. A Novel Implementation of Road Mapping from Digital Subtraction Angiography Images. In Proceedings of the CMBEBIH 2021, Mostar, Bosnia and Herzegovina, 21–24 April 2021.

5. Porumb, M.; Iadanza, E.; Massaro, S.; Pecchia, L. A convolutional neural network approach to detect congestive heart failure. *Biomed. Signal Process. Control.* **2020**, *55*, 101597. [CrossRef]

6. Neumuth, T. Surgical process modeling. *Innov Surg Sci* **2017**, *2*, 123–137. [CrossRef]

7. Hoetzenecker, K.; Chan, H.H.; Frommlet, F.; Schweiger, T.; Keshavjee, S.; Waddell, T.K.; Klepetko, W.; Irish, J.C.; Yasufuku, K. 3D Models in the Diagnosis of Subglottic Airway Stenosis. *Ann. Thorac. Surg.* **2019**, *107*, 1860–1865. [CrossRef]

8. Shi, C.; Sun, B.; Tang, G.; Xu, N.; He, H.; Ye, X.; Xu, G.; Gu, X. Clinical and radiological outcomes of endoscopic foraminoplasty and decompression assisted with preoperative planning software for lumbar foraminal stenosisSurgical process modeling. *Int. J. Comput. Assist. Radiol. Surg.* **2021**, *16*, 1829–1839. [CrossRef]

9. Maragiannis, D.; MS, J.; Igo, S.; Schutt, R.; Connell, P.; Grande-Allen, J.; Barker, C.; Chang, S.; Reardon, M.; Zoghbi, W.; et al. Replicating Patient-Specific Severe Aortic Valve Stenosis With Functional 3D Modeling. *Int. J. Comput. Assist. Radiol. Surg.* **2015**, *8*, e00362. [CrossRef]

10. Blankenhorn, D.H.; Kramsch, D.M. Reversal of atherosis and sclerosis. The two components of atherosclerosis. *Circulation* **1989**, *79*, 1–7. [CrossRef]

11. Sorelli, M.; Perrella, A.; Bocchi, L. Detecting vascular age using the analysis of peripheral pulse. *IEEE Trans. Biomed. Eng.* **2018**, *65*, 2742–2750. [CrossRef]

12. Selzer, R.H.; Mack, W.J.; Lee, P.L.; Kwong-Fu, H.; Hodis, H.N. Improved common carotid elasticity and intima-media thickness measurements from computer analysis of sequential ultrasound frames. *Atherosclerosis* **2001**, *154*, 185–193. [CrossRef] [PubMed]

13. Dobbe, J.G.; Streekstra, G.J.; Atasever, B.; Van Zijderveld, R.; Ince, C. Measurement of functional microcirculatory geometry and velocity distributions using automated image analysis. *Med. Biol. Eng. Comput.* **2008**, *46*, 659. [CrossRef] [PubMed]

14. Jamal, A.; Hazim Alkawaz, M.; Rehman, A.; Saba, T. Retinal imaging analysis based on vessel detection. *Microscopy research and technique* **2017**, *80*, 799–811. [CrossRef] [PubMed]

15. Kovács, G.; Hajdu, A. A self-calibrating approach for the segmentation of retinal vessels by template matching and contour reconstruction. *Med. Image Anal.* **2016**, *29*, 24–46. [CrossRef] [PubMed]

16. Sorelli, M.; Perrella, A.; Bocchi, L. Cardiac pulse waves modeling and analysis in laser doppler perfusion signals of the skin microcirculation. In Proceedings of the IFMBE Proceedings, Sarajevo, Bosnia and Herzegovina, 16–18 March 2017; Volume 62, pp. 20–25.

17. Rogai, F.; Manfredi, C.; Bocchi, L. Metaheuristics for specialization of a segmentation algorithm for ultrasound images. *IEEE Trans. Evol. Comput.* **2016**, *20*, 730–741. [CrossRef]

18. Simoni, A.; Tiribilli, E.; Lorenzetto, C.; Manetti, L.; Iadanza, E.; Bocchi, L. 3D Vessel Segmentation in CT for Augmented and Virtual Reality. In Proceedings of the Mediterranean Forum—Data Science Conference. Springer Computer Science, Sarajevo, Bosnia and Herzegovina, 24 October 2020. [CrossRef]

19. Babin, D.; Pižurica, A.; Velicki, L.; Matić, V.; Galić, I.; Leventić, H.; Zlokolica, V.; Philips, W. Skeletonization method for vessel delineation of arteriovenous malformation. *Comput. Biol. Med.* **2018**, *93*, 93–105. [CrossRef] [PubMed]

20. Kollmannsberger, P.; Kerschnitzki, M.; Repp, F.; Wagermaier, W.; Weinkamer, R.; Fratzl, P. The small world of osteocytes: Connectomics of the lacuno-canalicular network in bone. *New J. Phys.* **2017**, *19*, 073019. [CrossRef]
21. Felzenszwalb, P.F.; Huttenlocher, D.P. Distance transforms of sampled functions. *Theory Comput.* **2012**, *8*, 415–428. [CrossRef]
22. Barcali, E.; Iadanza, E.; Manetti, L.; Francia, P.; Nardi, C.; Bocchi, L. Augmented Reality in Surgery: A Scoping Review. *Appl. Sci.* **2022**, *12*, 6890. [CrossRef]
23. Vilser, W. Retinal vessel analyzer (RVA)-a new measuring system for examination of local and temporal vessel behaviour. *Investig. Ophthalmol. Vis. Sci.* **1997**, *38*, 678. [CrossRef]
24. Heneghan, C.; Flynn, J.; O'Keefe, M.; Cahill, M. Characterization of changes in blood vessel width and tortuosity in retinopathy of prematurity using image analysis. *Med. Image Anal.* **2002**, *6*, 407–429. [CrossRef] [PubMed]
25. Boskamp, T.; Rinck, D.; Link, F.; Kummerlen, B.; Stamm, G.; Mildenberger, P. New vessel analysis tool for morphometric quantification and visualization of vessels in CT and MR imaging data sets. *Radiographics* **2004**, *24*, 287–297. [CrossRef] [PubMed]
26. Nardi, C.; Salerno, S.; Molteni, R.; Occhipinti, M.; Grazzini, G.; Norberti, N.; Cordopatri, C.; Colagrande, S. Radiation dose in non-dental cone beam CT applications: A systematic review. *Radiol. Medica* **2018**, *123*, 765–777. [CrossRef] [PubMed]